

# Kinematic Analysis of the Deployable Truss Structures for Space Applications

Xu Yan<sup>1\*</sup>, Guan Fu-ling<sup>1</sup>, Zheng Yao<sup>1</sup>, Zhao Mengliang<sup>1,2</sup>

<sup>1</sup>Zhejiang University, Hangzhou – China

<sup>2</sup>Shanghai JiangNan Architectural Design Institute – China

**Abstract:** Deployable structure technology has been used in aerospace and civil engineering structures very popularly. This paper reported on a recent development of numerical approaches for the kinematic analysis of the deployable truss structures. The dynamic equations of the constrained system and the computational procedures were summarized. The driving force vectors of the active cables considering the friction force were also formulated. Three types of macroelements used in deployable structures were described, including linear scissor-link element, multiangular scissor element, and rigid-plate element. The corresponding constraint equations and the Jacobian matrices of these macroelements were formulated. The accuracy and efficiency of the proposed approach are illustrated with numerical examples, including a double-ring deployable truss and a deployable solar array.

**Keywords:** Kinematic analysis, Deployable truss structures, Macroelements, Deployable solar array.

## LIST OF SYMBOLS

$T$	Kinetic energy of the system;	$\alpha$	Half angle between the two active cable element nearby the point;
$X$	Generalized coordinate vector;	$\lambda$	Direction cosine of the cable element;
$M$	Inertia or mass matrix;	$\mu$	Dynamic friction coefficient;
$\dot{X}$	First order time derivative of X;	$\theta_k, \theta_{k-1}$	Start and end angle according to contact region;
$Q$	Vector that includes external and velocity dependent inertia force;	$\lambda_{ij}$	Direction cosine of the uniplate $ij$ .
$\Phi_i$	Geometrical constrain equations;		
$A$	Jacobian matrix of constrain equations;		
$h_1, h_2, \dots, h_p$	$p$ independent displacement modes of rigid-body movement;		
$\dot{a}$	Row vector consists on these combined coefficients in Eq. 6;		
$\rho$	Length density of the active cable;		
$T(\theta)$	Internal force vector;		
$f(\theta)$	Friction force vectors in the contact point;		
$N(\theta)$	Pressure force vectors in the contact point;		
$i, \ddot{i}$	Velocity and acceleration of cable length variety;		
$r$	Radius of the pulley;		

## INTRODUCTION

Deployable truss structures have been applied in many applications, such as solar arrays, masts and antennas (Meguro *et al.*, 2003) that have small-stowed volumes during launch, and are deployed by certain means to assume its predetermined shape accurately in orbit. Traditionally, a deployable truss structure consists of a large number of struts and kinematic pairs, which are simple, such as revolute joints, sliding hinges (Takamatsu and Onodaf, 1991), gears and pantograph struts (Cherniavsky *et al.*, 2005). This type of deployable structure has many advantages, including lighter weight, higher precision, smaller launch volume, and higher reliability for deployment.

There is a large amount of published literature on constrained rigid- and flexible-body dynamics, which focused on building the dynamic model, solving the differential equations and kinematic simulation. Many studies have

Received: 04/06/12 Accepted: 08/08/12

\*author for correspondence: xyzs@zju.edu.cn

School of Aeronautics and Astronautics/Zhejiang University, 38 Zheda Road – Xihu – Hangzhou, Zhejiang – China

only addressed simple beams and rigid bodies, which are not complicated deployable structures. Bayo and Ledesma (1996) presented a new integration method for constrained multibody dynamics. Fisetto and Vaneghem (1996) used the coordinate partitioning method of constrained Jacobian matrix to analyze the multibody system. An orthonormal tangent space method for constrained multibody systems was proposed by Blajer (1995), in which the independence basis vector of the tangent space of constrained surface needs to be calculated. Orthogonal matrix triangularization (QR decomposition) (Kim and Vanderploeg, 1986), singular value decomposition (Singh and Likins, 1985), and differentiable null space method (Liang and Lance, 1987) were used to obtain such basis vectors. Some authors have investigated the mechanism characteristics of deployable truss and tensegrity structures in their literatures (Calladine and Pellegrino, 1991; You, 2000). Bae *et al.* (2000) proposed an efficient implementation algorithm for real-time simulation of the multibody vehicle dynamics models. Newton chord method was employed to solve the equations of motion and constraints. Using the finite particle method (FPM), Yu and Luo (2009) presented a motion analysis approach of deployable structures based on the straight- and angulated-rod hinges. Kinematic and dynamic analysis, and control methods of the hoop truss deployable antenna were investigated by Li (2012).

This paper reports a recently-conducted effort that systematically addressed a kinematic analysis method of deployable truss structure based on macroelements, in which the friction force was considered.

## EQUATIONS OF MOTION CONSIDERING DRIVING CONDITIONS

### Dynamic equations for the constrained system

The dynamic equations for the constrained system and the computational procedures are summarized in this section. For the deployable spatial structure, the dependent Cartesian coordinates are used as generalized ones for the dynamic equation. The mass and velocity of the struts are reduced to two revolute joints at the two ends, and the kinetic energy of the system is defined as Eq. 1:

$$T = \frac{1}{2} \dot{X}^T M \dot{X} \quad (1)$$

where

$X$ : is the generalized coordinate vector, and

$M$ : is the inertia or mass matrix.

The first Lagrange equation is presented as Eq. 2:

$$(dX)^T \left( \frac{d}{dt} \frac{\partial T}{\partial \dot{X}} - \frac{\partial T}{\partial X} - Q \right) = 0 \quad (2)$$

where

$Q$ : is the vector that includes the external and velocity dependent inertia force,

$\dot{X}$ : is the first order time derivative of  $X$ .

By substituting Eq. 1 into 2, the dynamic equation can be determined as Eq. 3:

$$dX^T (M \ddot{X} - Q) = 0 \quad (3)$$

Because there are many complicated constrains in the deployable truss structures, the vector  $dX$ , according to the generalized coordinate vector, is dependent. Considering all types of constrains of the entire structures, the geometrical constrain equations are formulated as Eq. 4:

$$\Phi_i(X) = 0; i = 1, 2, \dots, s \quad (4)$$

Since all constrains of the deployable structure are constant with time  $t$  during the deployment process, the derivative of the constraint equations provide the Jacobian matrix (Eq. 5):

$$A \dot{X} = 0 \quad (5)$$

where

$A$ : is the corresponding Jacobian matrix of constraint equations.

The velocity equation (Eq. 5) is solved by the generalized inverse matrix method (Eq. 6):

$$\dot{X} = \dot{\alpha}_1 h_1 + \dot{\alpha}_2 h_2 + \dots + \dot{\alpha}_p h_p = H \dot{\alpha} \quad (6)$$

where

$h_1, h_2, \dots, h_p$ : are  $p$  independent displacement modes of the rigid-body movement,

$\dot{\alpha}$ : is a row vector that consists of these combined coefficients (Eq. 7).

$$\ddot{X} = H\ddot{\alpha} - A^+ \dot{A}\dot{X} \tag{7}$$

By replacing Eqs. 6 and 7 into the dynamic equation (Eq. 3), the following final dynamic equations are obtained (Eqs. 8 and 9):

$$\begin{aligned} \dot{X} &= H\dot{\alpha} \\ H^T M H \ddot{\alpha} - H^T M A^+ \dot{A} H \dot{\alpha} - H^T Q &= 0 \end{aligned} \tag{8}$$

With the initial condition:

$$X_{t=0} = X_0, \dot{X}_{t=0} = \dot{X}_0 \tag{9}$$

When the initial displacement and velocity vectors are known, the vector  $\dot{\alpha}_{t=0}$  in Eq. 6 can be obtained. By these initial values, Newmark's method is employed to solve the final dynamic equations (Eq. 8), therefore displacement, velocity, and acceleration of the deployable process in each time step can also be determined.

The numerical approach computational procedure is very simple and can be summarized as follows:

- all initial input dates of the entire structure and numerical simulation, such as the coordinates of the joints, structural topology, constraint conditions, driving mechanisms, boundary conditions and the length of time step, and so on, are provided;
- at any time step  $n$ , the mass matrix and driving force vectors are formed;
- the Jacobian matrix  $A$  and the first order derivative of the Jacobian matrix  $\dot{A}$  are formulated;
- the generalized inverse matrix and basis vector of null space of  $A$  are determined;
- if matrix  $A$  has full column, the rank will be estimated, if so go to the ninth step;
- the differential dynamic equations are calculated, and the displacement, velocity, and acceleration of all joints are obtained;
- update the positions of all joints and check whether the locked conditions of the structure is satisfied, if they are not, go to the second step; otherwise, go to the ninth step;
- if the period is less than the ending time, go to the second step, otherwise, the analysis should be stopped;
- the analysis is stopped and the output dates are ready for post process.

**Active cable driving and friction**

The purpose of this section is to formulate the driving force vectors of the active cables, which forms the term  $Q$  in the dynamic equations. Drive energy of the deployable truss structure comes from the electrical motor. When the active cables are driven by the motor, the cable length becomes shorter, and the structure is deployed. The driving forces in the active cables will become smaller after it loops over the pulley, so the Coulomb friction law is employed to consider the friction between the active cables and the pulley (Fig. 1).

The pretension force of the active cable in the free end is assumed as  $T_1$ . Considering the friction forces between the active cable and the pulley in the joints, driving forces of the cables in each deployable element are  $T_2, \dots, T_k, \dots, T_n$  in turn. Therefore, there are:  $T_1 > \dots > T_k > \dots > T_n$ .

The elastic deformations of the active cables are ignored, and a microarc element  $ds$  in the contact point between the cable and the pulley is analyzed, as shown in Fig. 1. The length density of the active cable is  $\rho$  and the internal force vector is denoted as  $T(\theta)$ . The friction and pressure force vectors in the contact point are denoted as  $f(\theta)$  and  $N(\theta)$ , respectively. The equilibrium equations of the microarc

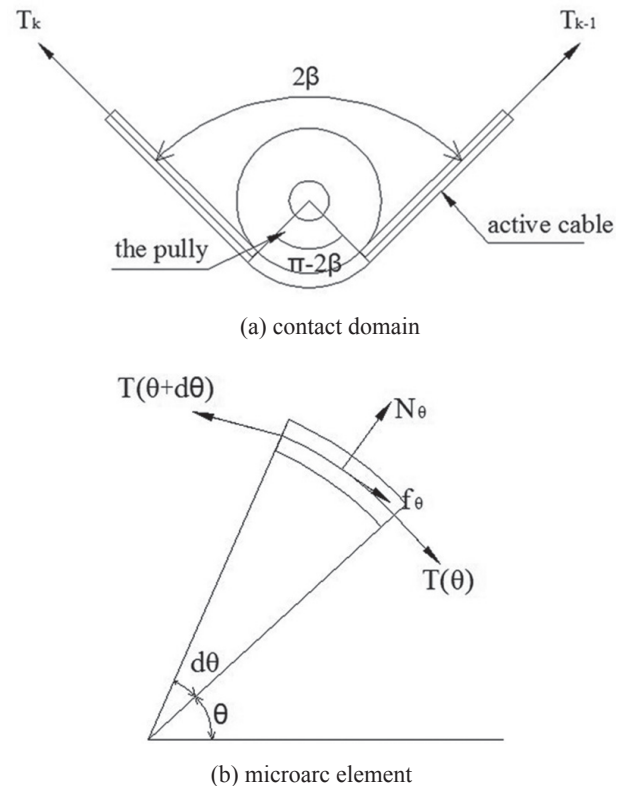


Figure 1. Active cable runs over a pulley.

element are obtained as in Eq. 10:

$$\begin{cases} T(\theta + d\theta)\cos d\theta - T(\theta) - f(\theta) = \rho ds \dot{l} \\ T(\theta + d\theta)\sin d\theta = N(\theta) + \rho ds \frac{\dot{l}^2}{r} \end{cases} \quad (10)$$

where

$\dot{l}$  and  $\ddot{l}$ : are the velocity and acceleration of cable length variety,  
 $r$ : is the radius of the pulley,

$\alpha$ : is the half angle between the two active cable elements nearby the point, as shown in Fig. 2.

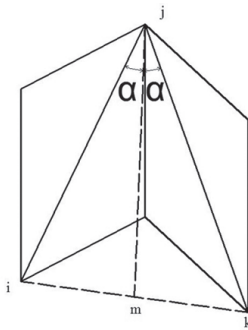


Figure 2. Active cables in two adjacent deployable elements.

Then, the velocity and acceleration of cable length variety  $\dot{l}$  and  $\ddot{l}$  were formulated. For the active cable element  $ij$  in a deployable element, the length can be expressed as Eq. 11:

$$[(X_i - X_j)^T (X_i - X_j)]^{\frac{1}{2}} = l \quad (11)$$

Differentiating Eq. 11 for the first and second times, Eqs. 12 and 13 were determined:

$$\dot{l} = \lambda(\dot{X}_j - \dot{X}_i) = [-\lambda \ \lambda] \begin{Bmatrix} \dot{X}_i \\ \dot{X}_j \end{Bmatrix} \quad (12)$$

$$\ddot{l} = [-\lambda^T \ \lambda^T] \begin{Bmatrix} \ddot{X}_i \\ \ddot{X}_j \end{Bmatrix} + [-\dot{\lambda}^T \ \dot{\lambda}^T] \begin{Bmatrix} \dot{X}_i \\ \dot{X}_j \end{Bmatrix} \quad (13)$$

where

$\lambda = \frac{1}{l} (X_j - X_i)^T$ : is the direction cosine of the cable element.

The Viscous and Coulomb friction laws can be combined into equations of motion, being the second one employed:

$$f(\theta) = \mu N(\theta) \quad (14)$$

where

$\mu$ : is the dynamic friction coefficient.

By utilizing the first equation of Eqs. 10 and 14, Eq. 15 is the result:

$$T(\theta + d\theta)\cos d\theta - T(\theta) - \mu \left[ T(\theta + d\theta)\sin \theta - \rho ds \frac{\dot{l}^2}{r} \right] = \rho ds \dot{l} \quad (15)$$

Then, there is Eq. 16:

$$\lim_{d\theta \rightarrow 0} \cos(d\theta) = 1, \quad \lim_{d\theta \rightarrow 0} \left( \frac{\sin d\theta}{d\theta} \right) = 1, \quad ds = R d\theta \quad (16)$$

Eq. 15 is divided by  $d\theta$  and the limit is gotten by  $d\theta \rightarrow 0$ . By using Eq. 16, it yields Eq. 17:

$$\frac{dT}{d\theta} = \mu T + (\rho r \dot{l} - \mu \rho l^2) \quad (17)$$

The start and end angles according to contact region are provided as  $\theta_k$  and  $\theta_{k-1}$ . The definite integral result of Eq. 17 is written as Eq. 18:

$$\int_{T_k}^{T_{k-1}} \frac{dT}{\mu T + (\rho r \dot{l} - \mu \rho l^2)} = \int_{\theta_k}^{\theta_{k-1}} d\theta \quad (18)$$

Solving such equations, it will yield Eq. 19:

$$\frac{\mu T_{k-1} + (\rho r \dot{l} - \mu \rho l^2)}{\mu T_k + (\rho r \dot{l} - \mu \rho l^2)} = e^{\mu(\theta_{k-1} - \theta_k)} \quad (19)$$

There is  $\theta_{k-1} - \theta_k = \pi - 2\beta$ , and the relation of the internal force of cable in two adjacent deployable elements can be obtained (Eq. 20):

$$\frac{\mu T_{k-1} + (\rho r \dot{l} - \mu \rho l^2)}{\mu T_k + (\rho r \dot{l} - \mu \rho l^2)} = e^{\mu(\pi - 2\beta)} \quad (20)$$

By utilizing Eq. 20, the friction force between the active cable and the pulley in the joint  $j$  is obtained (Eq. 21):

$$f_{k-1} = T_{k-1} - T_k \quad (21)$$

The generalized driving force of a driving cable element is as Eq. 22:

$$Q_c^e = \{Q_i^e \ Q_j^e\}^T \quad (22)$$

Such force of the vector  $Q$  of the entire structure is obtained by assembling the Eq. 22 for each element.

**JACOBIAN MATRICES OF THE MACROELEMENTS**

In this section, some deployable macroelements are investigated, and the corresponding Jacobian matrices are formulated. The equations of the constraints and the Jacobian matrices for a constant distance constraint on the members, the position constraint of the sleeve element, the angle constraint of the revolute joints and of synchronize gears have been presented in many references. For the sake of brevity, the formulations are not fully developed here, therefore see Nagaraj *et al.* (2009; 2010), Zhao and Guan (2005) for details.

**Linear scissor-link element**

Linear scissor-link element (SLE) is a type of fundamental macroelement in the deployable truss structures, where two pairs of struts are connected to each other at a pivot point O through a revolute joint, shown in Fig. 3. It allows two pairs of struts to rotate freely around the axis perpendicular to their common plane, but restrains all other degrees of freedom. At the same time, their endpoints are hinged to the ones of other elements.

As can be seen in Fig. 3, the angle between links *il* and *oi* is defined as the deploy angle  $\alpha$  of SLE. When the macroelement is deployed, this deploy angle becomes larger.

There are two constant distance constraint equations of the uniplets *ij* and *lk*, and the Jacobian matrix is formulated as Eq. 23:

$$A_i^e = \begin{bmatrix} -\lambda_{ij}^T & \lambda_{ij}^T & 0 & 0 \\ 0 & 0 & -\lambda_{kl}^T & \lambda_{kl}^T \end{bmatrix} \quad (23)$$

where the direction cosine of the uniplets *ij* is  $\lambda_{ij} = \frac{1}{L_{ij}}(X_j - X_i)$ , like the *kl* uniplets.

It is assumed that the length of *oi*, *ok* are *a* and the length of *oj*, *ol* are *k\*a*. Two pairs of uniplets are connected to each other at the point *o*. During the deployment process, the relative position of the connection point *o* is invariable. The

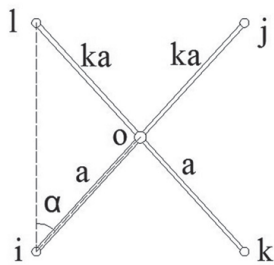


Figure 3. Linear scissor-link element.

constraint equation is as Eq. 24:

$$(X_i - X_j) \frac{a}{a(1+k)} + X_i = (X_k - X_l) \frac{a}{a(1+k)} + X_l \quad (24)$$

The upper equation is simplified to the following form (Eq. 25):

$$kX_i + X_j - kX_k - X_l = 0 \quad (25)$$

Differentiating it with respect to *X*, therefore the Jacobian matrix is obtained:

$$A_2^e = \{kI_{3 \times 3} \quad I_{3 \times 3} \quad -kI_{3 \times 3} \quad -I_{3 \times 3}\} \quad (26)$$

Because five revolute joints are coplanar during the deployment process, the planar equation is the constraint equations of the macroelement (Eq. 27).

$$(r_{ij} \times r_{ik}) \cdot r_{il} = 0 \quad (27)$$

When differences are compared with respect to *X*, the Jacobian matrix is obtained (Eq. 28):

$$A_3^e = \{(r_{il} \times r_{jk} - r_{ij} \times r_{ik})_{1 \times 3} \quad (r_{ik} \times r_{il})_{1 \times 3} \quad (r_{ij} \times r_{il})_{1 \times 3} \quad (r_{ij} \times r_{ik})_{1 \times 3}\} \quad (28)$$

For the planar SLE, the row number of the Jacobian matrix

$$Ae = \begin{Bmatrix} A_3^e \\ A_3^e \\ A_3^e \end{Bmatrix} \text{ is 6.}$$

**Planar multiangular scissor element**

Planar multiangular scissor element, as illustrated in Fig. 4, is another type of macroelement used in the deployable truss structures, in which the uniplets *ij* and *lk* are not aligned at an intermediate point *O*.

Based on the condition of two congruent triangles, the constraint equations of the planar multiangular scissor

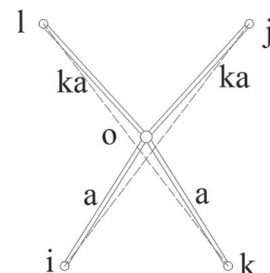


Figure 4. Planar multiangular scissor element.

element include:

- four truss members  $io, jo, ko$  and  $lo$  of the macroelement are considered and there are four constant distance constraint equations;
- two dummy truss members  $ij$  and  $lk$  are added to the macroelement; thus, there are two constant distance constraint equations;
- five points are coplanar, and the planar equation is constraint, which can be formulated by the same method as already mentioned.

For the planar multiangular scissor element, the row number of the Jacobian matrix  $A^e$  is eight.

**Rigid-plate element**

Planar rigid-plate element is a type of macroelement used in solar arrays. A four-node rigid plate element  $ijkl$  is shown in Fig. 5, which is connected to other members at corner points through a revolute joint.

The mass property of the macroelement is reduced to a finite number of points. The rigid-plate element is substituted with an equivalent grid of virtual rigid struts. The freedom degree of the element is analyzed: the degree of freedom of four spatial points  $i, j, k, l$  is 12. After the length constraints of six struts are appended, the total degree of freedom becomes six, which is equal to that of the rigid-plate element.

Six struts  $ij, jk, kl, li, ik$  and  $jl$  of the element are considered, and there are six constant distance constraint equations. For the planar-plate element, the row number of the Jacobian matrix  $A^e$  is six.

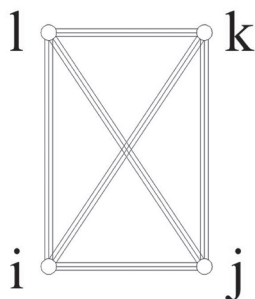


Figure 5. Rigid-plate element.

**NUMERICAL EXAMPLES**

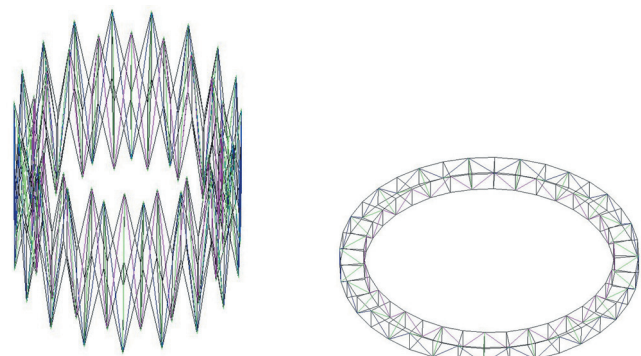
**Double-ring deployable truss**

A type of double-ring deployable truss based on quadrilateral elements is investigated for large-size mesh

antennas, the full deployed/folded configuration of which are shown in Fig. 6.

Two adjacent deployable elements of the outer and inner ring are shown in Fig. 7, which are quadrilateral elements with a diagonal sleeve element. The active cables pass through the diagonal sleeves. When the active cable is deployed by a motor and becomes shorter, the diagonal sleeves AE and CE contract. Then, the deployable elements are deployed. When the lengths of the diagonal sleeves AE and CE are equal to a designed value, the deployment of the elements is stopped.

Several planar truss elements can make a closed loop by arranging them side by side. The planar truss elements are also used in connecting the inner and outer loops. The structure topology is determined and the major design parameters of the truss are included: the side number of the ring is 18; the truss aperture is 5.0 m; the truss height is 0.5 m; the length of the chord struts in the outer ring is 0.8757 m; and the length of the chord struts in the inner ring is 0.6167 mm.



(a) deployed configuration (b) folded configuration  
Figure 6. Double-ring deployable truss.

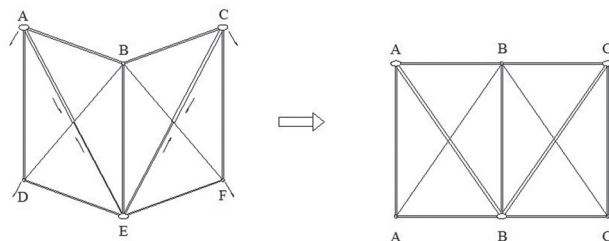


Figure 7. Deployment process of deployable truss elements.

The numbering of the truss joints is shown in Fig. 8. The motion process of the double-ring deployable truss was simulated by the program developed based on numerical approaches. The mass of each revolute joint is 0.25 kg.

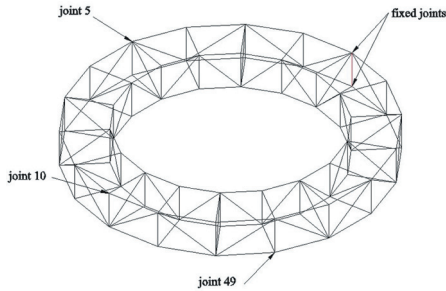


Figure 8. Numbering of the truss joints.

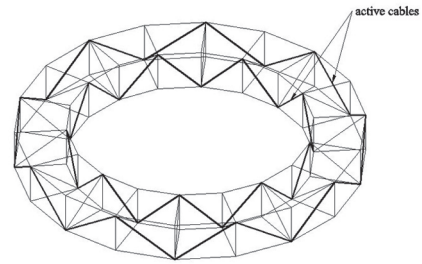


Figure 9. Active cables.

The active cables located in the model are shown in Fig. 9. The elastic deformations of the active cables are neglected and a constant 15 N driving force of the active cables in all configurations is assumed. To deploy the truss successfully, the dynamic friction coefficient  $\mu$  between the active cables and the pulley is required to be small, the real value of which is difficult to be measured. It is given to be a small default value 0.005 in this simulation work. The length of time step in the simulation is

0.05 second. The truss starts to move by active cables and reaches a static final configuration at last, which is shown in Fig. 10. When the lengths of the diagonal sleeves are equal to a designed value, the locked constraint conditions of the sleeves work and the simulation stops. It takes 102 seconds to be fully deployed. The coordinate variations of joints 5, 10 and 49 in the deployable truss are shown in Fig. 11, which can describe the variations of configurations during the structural motion in details.

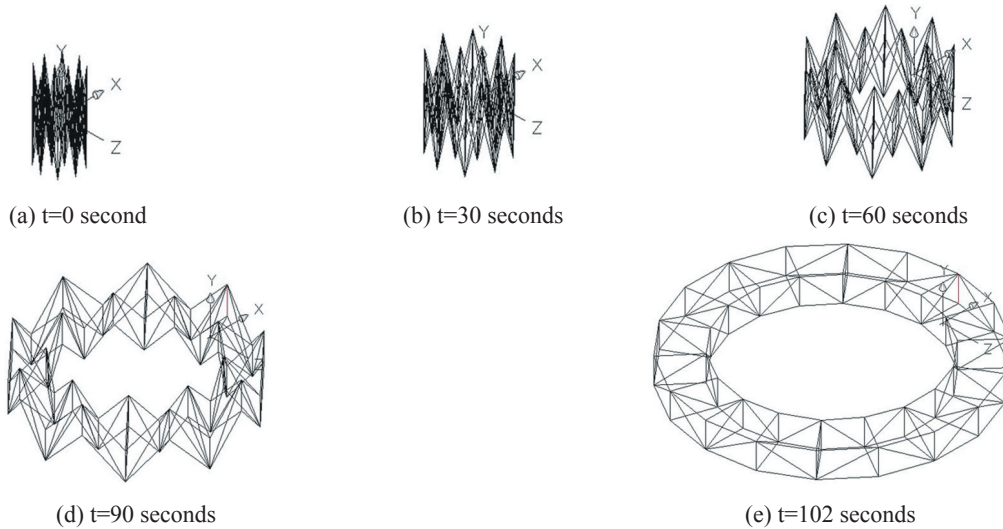
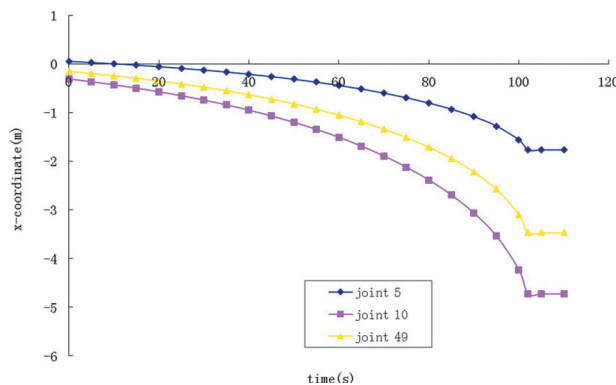
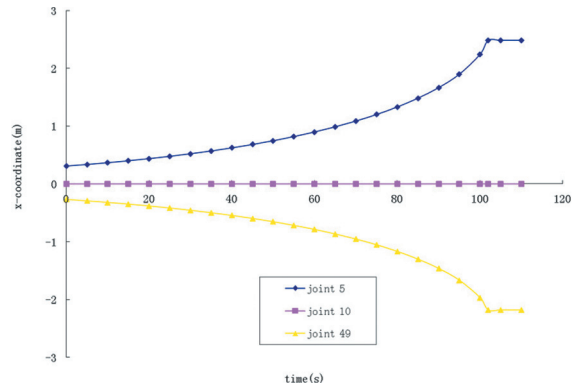


Figure 10. Motion process of the deployable truss.



(a) x axes coordinate



(b) y axes coordinate

Figure 11. Coordinate variations of joints 5, 10 and 49.

In the fully deployed configuration, the coordinates of points 5, 10, and 49 are respectively: (-1.771, 2.483, 0.681), (-4.730, 0, 0.691), and (-3.469, -2.184, 0.181). However, the reference coordinates of the deployed configuration, which are obtained from the geometric equation of this configuration, are (-1.763, 2.472, 0.6807), (-4.688, 0, 0.687), and (-3.469, -2.184, 0.181). The maximum error is 0.89%. Therefore, the method can simulate the motion behavior of the deployable truss effectively and accurately.

**Deployable sail arrays**

A scale model of deployable sail array based on SLEs is presented in Fig. 12. The sail array consists of eight SLE macroelements and eight rigid plate macroelements. The SLE macroelements are dynamic machines during deployment and support structure after deployment. The rigid plate elements are sail array deck, and these vertical struts such as 1-2 and 3-4 are sleeve element.

There are two active cables in the sail array, in which can be seen in Fig. 12. One of them, which is firmly connected to joint 25, runs over a pulley at joint 26, zigzags down the SLE following the route shown in the figure (it runs over a pulley at each kink) and, after passing over a pulley at joint 2, is connected to the motorized drum located below the base. The other active cable is arranged by the same method. The elastic deformation of the active cables is neglected, and a constant 10 N drive force of the active cables in all configurations is assumed.

Fixed boundary conditions are used at joints 1 and 4, and the translation along x direction of joints 2 and 3 are fixed. The

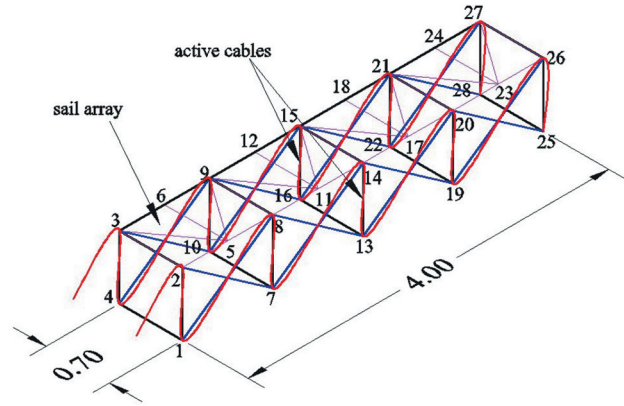


Figure 12. Scale model of the deployable sail array.

structure is deployed from the nearly flat configuration  $\alpha = 1.0^\circ$  to the final one  $\alpha = 55^\circ$ , as shown in Fig. 5. The mass of each revolute joint is 0.15 kg, and that of joints in the rigid plate macroelements is 0.075 kg. A time step  $dt = 0.05s$  is used in the simulation. The motion behavior of the sail array structure was simulated by the same program. The sail array starts to move by active cables and reaches a static final configuration, as shown in Fig. 13. When the lengths of the vertical sleeves are equal to a designed value, the locked constraint conditions of the sleeves work and the simulation stops.

The deployment time of the structure is 140 seconds. The coordinate variations of point 26 in this model with time are shown in Fig. 14, which can define the variations of configurations during the structural motion in details.

In the final completely deployed configuration, the coordinates of points 5, 26, and 28 are, respectively, (0.50092, 0, -0.00179), (4.00738, 0, -0.00181), and

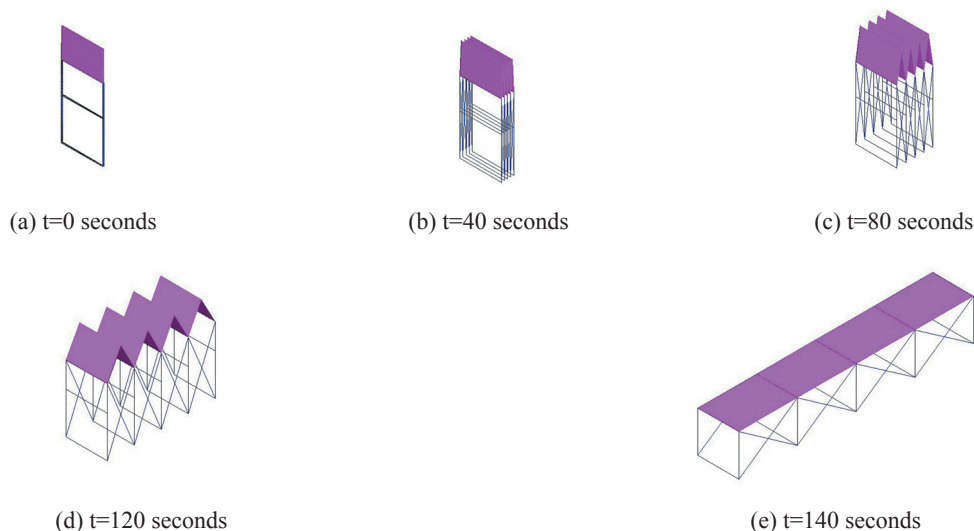


Figure 13. Motion process of the deployable sail arrays.

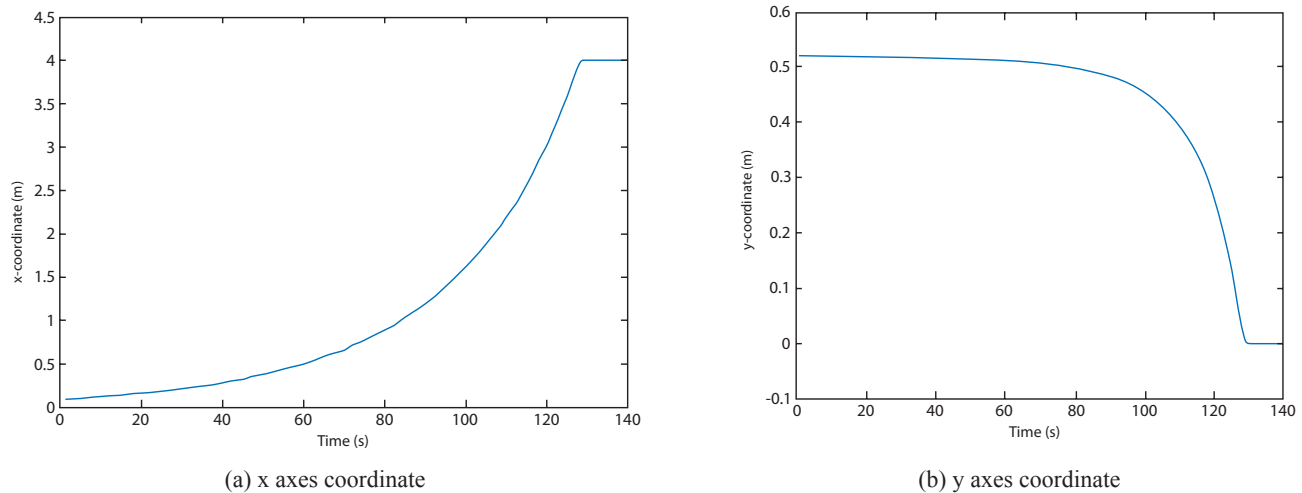


Figure 14. Coordinate variations of joint 26.

(4.00738, 0.7, -0.7), while the reference coordinates of these positions on the deployed configuration, which are obtained from the geometric equation of this configuration, are (0.50, 0, 0), (4.00, 0, 0), and (4.0, 0.7, -0.7). The maximum error is 0.18%. Therefore, the method can simulate the motion behavior of the deployable sail array effectively.

## CONCLUSIONS

This paper presents a numerical approach for kinematic analysis of the deployable truss structures. The driving forces of active cables are combined with the equations of motion. The friction between active cables and the pulley is considered. Three kinds of macroelements used in deployable structures are described. The corresponding constraint equations and Jacobian matrices of the macroelements are formulated. A double-ring deployable truss and a deployable solar array structure are selected as numerical examples. The deployment process and dynamic parameters at each time step can be simulated for evaluating the deployment behaviors of the structure. Results of the numerical simulation show that the capabilities of this method in the motion analysis are of complex deployable truss structures. The origin of the final error in the time step of the simulation is too large to stop the simulation nearby the reference configuration. To achieve higher simulation accuracy, the time step needs to be smaller.

Based on the researches included in this paper, future works are suggested: the reliability analysis of the deployment process can be researched; and deployment control of the deployable truss antennas needs to be investigated.

## REFERENCES

- Bae, D.S. *et al.*, 2000, "An explicit integration method for real time simulation of multibody vehicle models", *Computer Methods in Applied Mechanics and Engineering*, Vol. 187, pp. 337-350.
- Bayo, E. and Ledesma, R., 1996, "Augmented Lagrangian and mass-orthogonal projection method for constrained multibody dynamics", *Nonlinear Dynamics*, Vol. 9, pp. 113-130.
- Blajer, W., 1995, "An orthonormal tangent space method for constrained multibody systems", *Computer Methods In Applied Mechanics And Engineering*, Vol. 121, pp. 45-57.
- Calladine, C.R. and Pellegrino, S., 1991, "Further remarks on first-order infinitesimal mechanisms", *International Journal of Solids and Structures*, Vol. 29, pp. 2119-2122.
- Cherniavsky, A.G. *et al.*, 2005, "Large deployable space antennas based on usage of polygonal pantograph", *Journal of Aerospace Engineering*, Vol. 18, pp. 139-145.
- Fisette, P. and Vaneghem, B., 1996, "Numerical integration of multibody system dynamic equations using the coordinate partitioning method in an implicit Newmark scheme", *Computer Methods in Applied Mechanics and Engineering*, Vol. 135, pp. 85-105.

- Kim, S.S. and Vanderploeg, M.J., 1986, "QR decomposition for state space representation of constrained mechanical dynamic systems", *Journal of Mechanisms, Transmissions, and Automation in Design*, Vol. 108, pp. 183-188.
- Li, T.J., 2012, "Deployment analysis and control of deployable space antenna", *Aerospace Science and Technology*, Vol. 18, pp. 42-47.
- Liang, C.G. and Lance, G.M., 1987, "A differentiable null space method for constrained dynamic analysis", *Journal of Mechanisms, Transmissions, and Automation in Design*, Vol. 109, pp. 405-410.
- Meguro, A. *et al.*, 2003, "Key technologies for high-accuracy large mesh antenna reflectors", *Acta Astronautica*, Vol. 53, pp. 899-908.
- Nagaraj, B.P. *et al.*, 2009, "Kinematics of pantograph masts", *Mechanism and Machine Theory*, Vol. 44, pp. 822-834.
- Nagaraj, B.P. *et al.*, 2010, "A constraint Jacobian based approach for static analysis of pantograph masts", *Computers and Structures*, Vol. 88, pp. 95-104.
- Singh, R.P. and Likins, P.W., 1985, "Singular value decomposition for constrained dynamical systems", *Journal of Applied Mechanics*, Vol. 52, pp. 943-948.
- Takamatsu, K.A. and Onodaf, J., 1991, "New deployable truss concepts for large antenna structures or solar concentrators", *Journal of Spacecraft*, Vol. 28, pp. 330-338.
- You, Z., 2000, "Deployable structure of curved profile for space antennas", *Journal of Aerospace Engineering*, Vol. 13, pp. 139-143.
- Yu, Y. and Luo, Y., 2009, "Motion analysis of deployable structures based on the rod hinge element by the finite particle method", *Proceedings of the Institution of Mechanical Engineers, Part G: Journal of Aerospace Engineering*, Vol. 223, pp. 955-965.
- Zhao, M.L. and Guan, F.L., 2005, "Kinematic analysis of deployable toroidal spatial truss structures for large mesh antenna", *Journal of the International Association for Shell and Spatial Structures*, Vol. 46, pp. 195-204.